JGR Biogeosciences

RESEARCH ARTICLE
10.1029/2020JG005977

**Key Points:**

- Molecular composition indicated minimal inputs of microbially unaltered permafrost thaw dissolved organic carbon (DOC) into the Kolyma River
- Thermochemical composition and radiocarbon ages indicated minimal inputs of 28-days microbially degraded permafrost thaw DOC
- No directly permafrost-aged component was evident in underlying age structure of Kolyma River DOC

**Supporting Information:**

Supporting Information may be found in the online version of this article.

**Correspondence to:**

J. A. Rogers,
jar15h@my.fsu.edu

**Citation:**

Rogers, J. A., Galy, V., Kellerman, A. M., Chanton, J. P., Zimov, N., & Spencer, R. G. M. (2021). Limited presence of permafrost dissolved organic matter in the Kolyma River, Siberia revealed by ramped oxidation. *Journal of Geophysical Research: Biogeosciences*, *126*, e2020JG005977. https://doi.org/10.1029/2020JG005977

Received 26 JUL 2020
Accepted 29 JUN 2021

**Author Contributions:**

**Conceptualization:** Jennifer A. Rogers, Valier Galy, Jeffrey P. Chanton, Robert G. M. Spencer
**Formal analysis:** Jennifer A. Rogers, Valier Galy, Anne M. Kellerman
**Funding acquisition:** Jeffrey P. Chanton, Robert G. M. Spencer
**Investigation:** Jennifer A. Rogers, Valier Galy, Anne M. Kellerman
**Methodology:** Jennifer A. Rogers, Valier Galy, Robert G. M. Spencer
**Project Administration:** Jennifer A. Rogers, Robert G. M. Spencer
**Resources:** Valier Galy, Nikita Zimov, Robert G. M. Spencer
**Software:** Jennifer A. Rogers, Valier Galy, Anne M. Kellerman



# Limited Presence of Permafrost Dissolved Organic Matter in the Kolyma River, Siberia Revealed by Ramped Oxidation

**Jennifer A. Rogers[1], Valier Galy[2], Anne M. Kellerman[1], Jeffrey P. Chanton[1], Nikita Zimov[3], and Robert G. M. Spencer[1]**

[1]National High Magnetic Field Laboratory Geochemistry Group and Department of Earth, Ocean, and Atmospheric Science, Florida State University, Tallahassee, FL, USA, [2]Woods Hole Oceanographic Institution, Woods Hole, MA, USA, [3]Northeast Science Station, Far East Branch of Russian Academy of Sciences, Cherskiy, Russia

**Abstract** Increasing Arctic temperatures are thawing permafrost soils and liberating ancient organic matter, but the fate of this material remains unclear. Thawing of permafrost releases dissolved organic matter (DOM) into fluvial networks. Unfortunately, tracking this material in Arctic rivers such as the Kolyma River in Siberia has proven challenging due to its high biodegradability. Here, we evaluate late summer abruptly thawed yedoma permafrost dissolved organic carbon (DOC) inputs from Duvannyi Yar. We implemented ultrahigh-resolution mass spectrometry alongside ramped pyrolysis oxidation (RPO) and isotopic analyses. These approaches offer insight into DOM chemical composition and DOC radiocarbon values of thermochemical components for a permafrost thaw stream, the Kolyma River, and their biodegraded counterparts ($n = 4$). The highly aliphatic molecular formula found in undegraded permafrost DOM contrasted with the comparatively aliphatic-poor formula of Kolyma River DOM, represented by an 8.9% and 2.6% relative abundance, respectively, suggesting minimal inputs of undegraded permafrost DOM in the river. RPO radiocarbon fractions of Kolyma River DOC exhibited no "hidden" aged component indicative of permafrost influence. Thermostability analyses suggested that there was limited biodegraded permafrost DOC in the Kolyma River, in part determined by the formation of high-activation energy (thermally stable) biodegradation components in permafrost DOM that were lacking in the Kolyma River. A mixing model based on thermostability and radiocarbon allowed us to estimate a maximum input of between 0.8% and 7.7% of this Pleistocene-aged permafrost to the Kolyma River DOC. Ultimately, our findings highlight that export of modern terrestrial DOC currently overwhelms any permafrost DOC inputs in the Kolyma River.

**Plain Language Summary** Climate change is warming the Arctic faster than anywhere on Earth. Permafrost, or frozen soil, contains a vast amount of carbon locked in an icy repository. With warming temperatures, permafrost is thawing, and this thawed organic material can be transformed by microbes into greenhouse gases, leading to further warming. The amount of permafrost thawing into rivers, however, has been difficult to determine. In this study, we examined material in both permafrost thaw water, and thaw water material degraded by microbes, then compared it to material in a major Arctic river to see if we can find a sign of permafrost inputs. Permafrost is also very old and this old carbon mixes with modern sources of carbon in the river. We used a new analytical technique to see if we could find old carbon derived from permafrost in the river during late summer when permafrost thaw inputs are greatest. Even with the novel approach, we found little evidence of old carbon, suggesting that major Arctic rivers are currently only exporting a limited amount of permafrost carbon to the Arctic Ocean. This research highlights that the exported carbon is predominantly from plants and other contemporary sources within the watershed.

## 1. Introduction

Temperatures in the Arctic are increasing at twice the global average rate of warming (IPCC, 2013). Efforts to quantify the amount and fate of permafrost dissolved organic carbon (DOC) input into major Arctic rivers are increasingly important as the Arctic warms and permafrost thaw rates increase. Permafrost soils in the Arctic hold approximately twice as much carbon as the atmosphere at an estimated 1,330–1,580 Pg within

**Supervision:** Valier Galy, Anne M. Kellerman, Jeffrey P. Chanton, Nikita Zimov, Robert G. M. Spencer
**Validation:** Jennifer A. Rogers, Valier Galy, Anne M. Kellerman, Robert G. M. Spencer
**Visualization:** Jennifer A. Rogers, Anne M. Kellerman, Robert G. M. Spencer
**Writing – original draft:** Jennifer A. Rogers
**Writing – review & editing:** Jennifer A. Rogers, Valier Galy, Anne M. Kellerman, Jeffrey P. Chanton, Robert G. M. Spencer

surface soils (<3 m), river deltas (>3 m), and deep yedoma deposits (>3 m) (Schuur et al., 2015). The Kolyma River watershed in northeastern Siberia, with an area of 650,000 $km^2$, is the sixth-largest Arctic watershed, and the world's largest watershed entirely underlain by continuous permafrost (Holmes et al., 2012). The Kolyma River encompasses extensive regions of yedoma permafrost or ice complex deposits, which formed in areas that remained unglaciated during the Pleistocene, accreting biomass and accumulating fine silts (Schirrmeister et al., 2002). Yedoma permafrost is defined by its high ice (~80% average volume) and organic carbon (OC) content (2.5%–3% average C by mass) (Strauss et al., 2013, 2017; Zimov et al., 2006). The yedoma region alone is estimated to account for ~210–~456 Pg of global permafrost C storage (Anthony et al., 2014; Strauss et al., 2013).

Assessing how permafrost thaw DOC is contributing to, and changing with respect to Arctic riverine export, has been the focus of numerous recent studies (Bowen et al., 2020; Drake et al., 2018; Ewing et al., 2015; Mann et al., 2015; Rocher-Ros et al., 2020; Spencer et al., 2015; Wickland et al., 2018). Abrupt thaw through thermokarst formation including thaw slumps has shown to be a major contributor of permafrost carbon release with a lasting impact on aquatic carbon concentrations (Abbott et al., 2014, 2015; Turetsky et al., 2020). Kolyma River yedoma is predicted to release larger quantities in this form due to its high ice content (Strauss et al., 2017; Wild et al., 2019). However, mobilization and export of permafrost DOC into fluvial networks are obscured by dynamic introduction pathways, such as scattered ephemeral permafrost thaw streams interspersed with mass wasting events of variable spatial distributions (Abbott et al., 2015; Vonk et al., 2013).

Ultimately, the fate of permafrost DOM is tied to its composition which is linked to how the permafrost formed as well as past thaw modification, with different permafrost endmembers showing marked DOM compositional variability (MacDonald et al., 2021; Spencer et al., 2015; Ward & Cory, 2016). DOC in streams thawing from yedoma permafrost in the Kolyma Basin is $^{14}C$ depleted (~20,000 $^{14}C$ yBP old) and exhibits an exceedingly aliphatic (high H/C) dissolved organic matter (DOM) compositional signature (Spencer et al., 2015; Stubbins et al., 2017). Bioincubations of yedoma permafrost have shown large (>50%–60%) decreases in DOC concentration over 28 days, indicating its high biolability (Spencer et al., 2015). However, with a Kolyma River residence time from thaw streams to the ocean of only 3–7 days, it seems reasonable that permafrost derived DOC would still be detectable at the mouth of the Kolyma River (Drake et al., 2018; Spencer et al., 2015; Vonk et al., 2013). Despite this, modern bulk DOC radiocarbon age at the mouth of the Kolyma River suggests limited permafrost DOC export to the Arctic Ocean (Spencer et al., 2015; Vonk et al., 2013). Two scenarios could explain this phenomenon, either: (a) a considerable quantity of the permafrost derived DOC is rapidly degraded between source and export to the sea (i.e., the mouth of the Kolyma River) or (b) the permafrost DOC contribution at the mouth of the Kolyma River is overwhelmed by modern DOC inputs (i.e., modern DOC inputs dominate the Kolyma River).

In this study, we focused on the role of microbial degradation on permafrost DOM, as past studies have highlighted the extreme biolability and low photolability of yedoma DOM in the Kolyma Basin (Mann et al., 2015; Spencer et al., 2015; Stubbins et al., 2017). Biodegraded yedoma permafrost has a DOM molecular-level signature similar to that of the Kolyma River mainstem, thus complicating efforts to trace permafrost inputs in the bulk DOM pool (Drake et al., 2018; Spencer et al., 2015). Similarly, because bulk radiocarbon ($\Delta^{14}C$-DOC) values represent the average $^{14}C$ age of all contributing C sources, a modern bulk $^{14}C$ age can mask minor inputs of aged permafrost carbon (Mann et al., 2015). Ramped pyrolysis oxidation (RPO) coupled with isotopic analyses strives to tease apart composite DOC source and age in an attempt to solve this problem (Hemingway et al., 2019; Rosenheim et al., 2013; Williams et al., 2015). In short, RPO is the process of combusting a sample at steadily increasing temperatures and trapping the $CO_2$ released. RPO then assesses the stable ($\delta^{13}C$-DOC) and radiocarbon isotopic values of sample gas fractions taken across user-defined thermal intervals, covering the entire spectrum of thermal reactivity. This technique allows radiocarbon assignments to components thermally oxidized at variable temperatures.

A negative relationship between bioavailability and thermostability has been shown where thermally stable material was less available for microbial respiration (Leifeld & von Lützow, 2014). Thus, $CO_2$ generated across these temperature intervals relates to its thermostability, a proxy for biological reactivity and the theoretical barrier to energy acquisition (i.e., activation energy [$E$]). In particular, thermal parameters have shown to be a useful measure of aromaticity, where low H/C compounds are preferentially found at higher

temperature values (De la Rosa et al., 2008, 2018; Peltre et al., 2013; Sanderman & Grandy, 2020). Microbes degrade and uptake a range of DOM, though relatively high H/C material is thought to be more biolabile (D'Andrilli et al., 2015; Šantl-Temkiv et al., 2013; Spencer et al., 2015), and biolability has been shown to positively correlate with the abundance of aliphatic compounds (Textor et al., 2019).

We paired RPO with Fourier transform ion cyclotron resonance mass spectrometry (FT-ICR MS) because of its unparalleled insights into the molecular composition of complex mixtures such as DOM (Kujawinski, 2002; Kurek et al., 2020; Stubbins et al., 2010). Additionally, for RPO analyses, this study utilized *E* as opposed to temperature as it is a more objective proxy for chemical composition (Hemingway, Rothman, et al., 2017). Because of the correlation between aliphatic content and biolability, we can then expect that the highly bioavailable low aromatic component of permafrost should be oxidized at low temperature, that is, have a low *E*. Hence, if the Kolyma River mainstem contains a non-biologically degraded permafrost DOM component masked at the bulk level by modern DOC inputs, we hypothesize that it will manifest itself as a $^{14}$C-depleted low *E* component similar to undegraded permafrost DOC. Alternatively, if the Kolyma River mainstem contains biodegraded permafrost, we would expect to see a hidden aged fraction of OC at a thermal interval similar to that of biodegraded permafrost DOC. Ultimately, our aim here is twofold. First, we examined if coupled RPO and isotopic analysis can separate a distinct, aged permafrost thaw component within the modern bulk DOC age of the Kolyma River mainstem. Second, we examined whether bioincubation of permafrost thaw water results in a shift in thermostability (as determined by RPO) toward that of the Kolyma River (e.g., from low *E* to higher *E*) accompanied by a loss of its uniquely aliphatic molecular composition as seen by FT-ICR MS. This loss in distinctive formula has been observed previously in biodegraded permafrost DOM (Spencer et al., 2015). Thus, from a DOM compositional standpoint, biodegraded permafrost thaw DOM would become difficult to distinguish from Kolyma River mainstem DOM but would retain its old $^{14}$C age. Overall, this study serves to elucidate the potential flux and fate of permafrost thaw DOC integrating into the Kolyma River, as well as add to growing research on the thermostability of DOC in riverine systems.

## 2. Methods

### 2.1. Sample Collection and Bioincubations

To investigate the relationship between permafrost thaw DOM and Kolyma River mainstem DOM, water was collected from a permafrost thaw stream at Duvannyi Yar, a permafrost erosion site (68°37′48″N, 159°9′3.6″E), and the Kolyma River (68°47′6″N, 161°20′9.6″E) outside of Cherskiy, Russia (Figure 1). Samples were collected in late August 2018 when the thaw depth of the active layer is deepest, and consequently permafrost thaw is expected to be at its highest (Schuur et al., 2008). Water samples were collected in acid-washed high-density polyethylene bottles and filtered through precombusted (450°C > 5 h) 0.7 μm glass fiber filters. A set of samples for DOC concentration, RPO, and FT-ICR MS were immediately frozen (−20°C) before any microbial degradation could occur (hereafter referred to as t0). Immediately after filtration, permafrost thaw water and Kolyma River water were incubated with the microbial consortia that remained post 0.7 μm filtration following the protocols of Vonk et al. (2015). Bioincubations were kept in the dark at 20°C for 28 days following established protocol (Spencer et al., 2015; Vonk et al., 2013). Bottles were periodically allowed to ventilate and re-equilibrate with atmospheric $O_2$ concentrations, followed by perturbation by inversion to prevent anoxia. Bioincubations were terminated by filtration through a precombusted (450°C > 5 h) 0.7 μm glass fiber filter and frozen immediately (−20°C). Henceforth, Kolyma River and permafrost before bioincubation will be referred to as Kolyma River (t0) and undegraded permafrost (t0), and post-biodegradation as Kolyma River (t28) and degraded permafrost (t28).

### 2.2. Dissolved Organic Carbon Analyses

DOC concentration was analyzed using the non-purgeable OC method on a Shimadzu total organic carbon (TOC-L) CPH analyzer with all samples acidified to pH 2 and sparged with zero-grade air for 5 min to remove dissolved inorganic carbon. Potassium hydrogen phthalate, or KHP, was used to create calibration curves to encompass the range of DOC sample concentrations. All DOC concentration analyses had

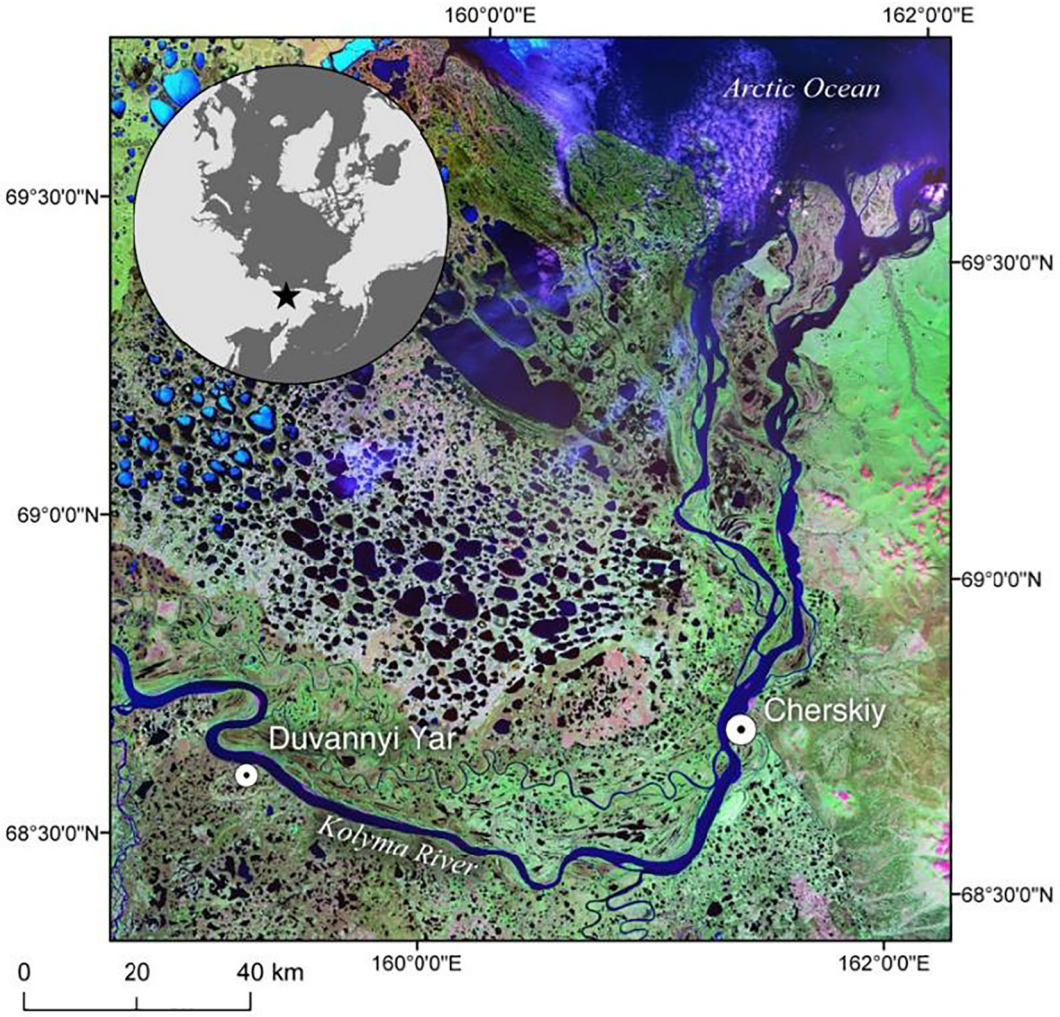


**Figure 1.** A map of the study sites in the Kolyma River watershed. Permafrost thaw water was collected from Duvannyi Yar, and Kolyma River water was collected at Cherskiy.

a coefficient of variance <2% and are reported in mg $L^{-1}$. BDOC is the percent biolabile component or the expression of DOC percent loss after a 28-days period as defined by Vonk et al. (2015).

### 2.3. Ultrahigh-Resolution Mass Spectrometry

FT-ICR MS offers unmatched insight into complex mixtures of DOM because of its high mass accuracy and capability to distinguish molecular formula (Hendrickson et al., 2015; Kurek et al., 2020). In short, samples were first extracted by concentration and purification through a 100 mg PPL resin (Agilent Bond Elute) cartridge (Dittmar et al., 2008). For this solid phase extraction, DOC concentration was used to calculate the volume necessary to extract 40 μg of OC. The cartridges maintained the DOM until eluted with 1 mL of high-grade methanol into precombusted (550°C > 5 h) amber vials with methanol-cleaned caps. Methanol eluates were stored at −20°C until analyzed at the National High Magnetic Field Laboratory (NHMFL) in Tallahassee, FL, USA. Each sample was introduced into the 9.4-tesla FT-ICR MS instrument after being negatively ionized using electrospray ionization (ESI). Mass to charge ratios created mass spectra that detected measurement within the range of 170–1,000 m/z while excluding noise at a ratio below baseline plus six times the root mean squared baseline (O'Donnell et al., 2016). The mass spectra were calibrated and processed with the use of the modular ion cyclotron resonance data acquisition system (Blakney et al., 2011) and PetroOrg©,™ software (developed by Yuri E. Corilo) (Corilo, n.d.) engineered at the NHMFL. Chemical

formula were assigned using a combination of the following elemental ranges: $C_{1–45}$, $H_{1–92}$, $N_{0–4}$, $O_{1–25}$, and $S_{0–2}$. Based on these formula and their modified aromaticity indices ($AI_{mod}$), defined by Koch and Dittmar (2006, 2016), each is sorted into operationally defined compound classes according to the following specifications: aliphatic (H/C ≥ 1.5, O/C < 0.9, $N = 0$); condensed aromatic ($AI_{mod} > 0.67$); polyphenolic ($AI_{mod}$ 0.50–0.67); highly unsaturated and phenolic (HUP) high oxygen ($AI_{mod} < 0.5$, H/C < 1.5, O/C ≥ 0.5); HUP low oxygen ($AI_{mod} < 0.5$, H/C < 1.5, O/C < 0.5); and peptide-like (H/C ≥ 1.5, O/C < 0.9, $N \geq 1$) (O'Donnell et al., 2016). With respect to the definition of compounds used here, it is noted that molecular formula can present themselves as multiple isomers, and we refrain from inferring structure.

### 2.4. Ramped Pyrolysis Oxidation Coupled Radiocarbon Analysis

RPO coupled with stable and radiocarbon analyses was performed on all samples following the established methodology of Rosenheim et al. (2008), modified for liquid samples. All samples were prepared for RPO analysis using the same solid phase extraction process as for FT-ICR MS, albeit with the aim of extracting 1 mg of OC. The cartridges maintained the DOM until eluted with 1 mL of high-grade methanol into pre-combusted (550°C > 5 h) amber vials with methanol-cleaned caps. Eluates were stored at −20°C. Subsequently, the methanol extracts were evaporated down at a minimally elevated temperature under flowing $N_2$ gas before undergoing thermal fractionation: the DOC in the reaction chamber was converted to $CO_2$ during a continuous ramp rate of 5°C per minute. Set on oxidation mode, this constant stream of helium containing ∼8% oxygen carries the combustion products downstream where the temperature is held at 800°C, and nickel, copper, and platinum catalyze the complete conversion of the combustion products into $CO_2$ (Hemingway, Galy, et al., 2017). The $CO_2$ concentration in the carrier gas is then measured using an infrared gas analyzer (IRGA) to create a thermogram, with evolved $CO_2$ concentration as a function of temperature. Trapping for each sample began at ∼125°C, to ensure no methanol from the extraction process remained, nevertheless $CO_2$ generation remained near the baseline at temperatures <125°C. $CO_2$ aliquots were captured in toggled traps then cryogenically processed using slurries of isopropanol and dry ice to remove water and noncondensables on a vacuum line, until an adequate quantity was produced for both stable and radiocarbon analysis then flame sealed in borosilicate glass ampules. The $CO_2$ amount of each fraction was determined manometrically. Four to five fractions were collected for each sample. All quartz glassware used in this study was pre-combusted (850°C > 5 h) before use. Moreover, to estimate thermogram reproducibility, the Kolyma River (t0) sample was analyzed twice. No changes to distribution or shape were noted. Successive data transformation into $E$ distributions ensures that slight changes in analytical conditions (e.g., ramp rate) will not alter results (Hemingway, Rothman, et al., 2017), thus, collectively supporting the need for no further replicate runs.

For each fraction, 10% of the gas was used for stable C isotopic analysis (reported as $\delta^{13}C$ values) on a dual-inlet isotope ratio mass spectrometer while the remainder was converted to graphite using the Fe-$H_2$ method in preparation for $^{14}C$ measurements on an accelerator mass spectrometer located at the National Ocean Sciences Accelerator Mass Spectrometry (NOSAMS) facility in Woods Hole, MA. The Fm notation is used here in place of $F^{14}C$ as proposed by Reimer et al. (2004). Isotopic practices follow those of NOSAMS and the reporting of Stuiver (1980) and Stuiver and Polach (1977) and were consistent with previous studies utilizing RPO (Hemingway et al., 2018, 2019).

Bulk $\delta^{13}C$-DOC values from PPL extracts were also collected to correct for blank and kinetic fractionation inherent to the RPO process (Hemingway, Rothman, et al., 2017). For some gas fractions, we were unable to measure the stable isotope composition; in that case, $\delta^{13}C$ values were back calculated using mass balance approaches. First, the missing value was constrained to those that would limit offset from the bulk $\delta^{13}C$-DOC to that of the maximum and minimum offset in the remaining samples. This was then further constrained to values that would not exceed the maximum and minimum range past that of the remaining sample sets. The average of these values and its uncertainty were used in place of missing values. When propagating the weighted average error for both Fm and $\delta^{13}C$ values, a 5% uncertainty on fraction sizes was included to offer a robust assessment of error following the recommendations of Hemingway, Galy, et al., 2017.

**Table 1**
*Dissolved Organic Carbon Concentrations and Chemical Composition of Each Sample*

| Sample | Incubation period (Days) | DOC (mg $L^{-1}$) | BDOC (%) | Assigned formula (#) | Mass (Da) | $AI_{mod}$ | HUP high O/C (%RA) | HUP low O/C (%RA) | Polyphenolic (%RA) | Condensed aromatic (%RA) | Aliphatic (%RA) | Peptide-like (%RA) |
|---|---|---|---|---|---|---|---|---|---|---|---|---|
| Kolyma River | 0 | 3.9 | – | 7,605 | 476.3 | 0.313 | 60.7 | 27.5 | 7.5 | 1.3 | 2.6 | 0.4 |
| Kolyma River | 28 | 3.8 | 2.6 | 7,528 | 479.7 | 0.313 | 59.5 | 28.2 | 7.8 | 1.3 | 2.7 | 0.5 |
| Permafrost | 0 | 112.8 | – | 8,385 | 430.6 | 0.293 | 61.3 | 17.1 | 7.4 | 4.1 | 8.9 | 1.3 |
| Permafrost | 28 | 67.5 | 40.2 | 9,072 | 449.6 | 0.296 | 67.3 | 17.5 | 6.9 | 3.3 | 4.2 | 0.8 |

*Note*. Biolabile dissolved organic carbon (BDOC) is the percent loss after 28-days bioincubations. Here %RA is the percent relative abundance of a compound class. HUP compounds are highly unsaturated and phenolic. The mass and AImod are the calculated weighted averages.
Abbreviation: HUP, highly unsaturated and phenolic.

### 2.5. Inverse Modeling Activation Energy Distribution

Thermograms were graphed from IRGA data, where $CO_2$ is presented as a function of temperature, or time, as they are linearly related. Thermograms were transformed into non-parametric *E* distributions following the inverse model of Hemingway, Rothman, et al. (2017, 2018). Noise, at a scale of analytical uncertainty, is smoothed to remove instrument measurement artifacts. Then, thermograms were inversely modeled to generate a probability density function where carbon is related to the *E* necessary to oxidize the carbon atom into $CO_2$. In theory, the decay process follows the probability density function producing the obtained thermogram (Hemingway, Rothman, et al., 2017). $p(0,E)$ then is the distribution of *E*, denoting the fraction of the total C initially associated with an *E* value, where the area under the curve integrates to 1. This method departs from assuming the probability density function of decay products as Gaussian or normally distributed. This method allows the comparison of samples across varying ramp rates (°C $min^{-1}$), reinforcing uniformity in the analytical process. This modeling approach ultimately allows us to quantitatively attribute *E* to carbon bond strength and can be implemented as a proxy for physio-chemical composition (Hemingway, 2018; Hemingway, Rothman, et al., 2017). Through our modeling approach, the fractions overlap in *E* space, along with their isotopic composition, representing fractions as mixtures of varying components.

During the regularization process, or thermogram smoothing step in the inverse model, because our DOC samples did not automatically present a maximum curvature for the best fit regularization weighting factor, $\lambda$, it was set at 0.5 in an attempt to balance the residual error and roughness (Hemingway, Rothman, et al., 2017). The Arrhenius pre-exponential factor, Ω, remained at $10^{10}$ $s^{-1}$, as prescribed in Hemingway, Rothman, et al. (2017). Samples were additionally blank and fractionation corrected at this time. Hemingway et al. (2018) implemented this inverse RPO approach to effectively support a hypothesis of increased biodegradation and $CO_2$ production from stored aged OC in mountain range soils as they undergo erosion. Endmembers were relatively constrained to *E*-range groupings as radiocarbon values follow suit, and thus, it is a fitting approach for the goals of this study.

## 3. Results

### 3.1. DOC Biolability and DOM Chemical Composition

The aerobic bioincubations of permafrost DOC saw a 40.2% loss from 112.8 to 67.5 mg $L^{-1}$ over 28 days at 20°C. This is similar to previous studies that found BDOC values ranging from 29.9% to 68.8% after 28 days of incubation for permafrost thaw DOC at this site (Mann et al., 2015; Spencer et al., 2015; Vonk et al., 2013). Comparatively, after incubation we observed a loss of Kolyma River DOC (2.6%) from 3.9 to 3.8 mg $L^{-1}$ (Table 1), again comparable to the losses shown in previous studies for this location (Mann et al., 2015; Spencer et al., 2015).

FT-ICR MS highlights pronounced changes in permafrost DOM composition post-biodegradation (t28) (Figure 2 and Table 1). The largest change was seen as an increase in the percent relative abundance of the high O/C HUP compounds from 61.3% to 67.3%. The largest comparative change was seen in aliphatic compounds, which decreased by more than half from 8.9%RA to 4.2%RA after biodegradation (Figure 2

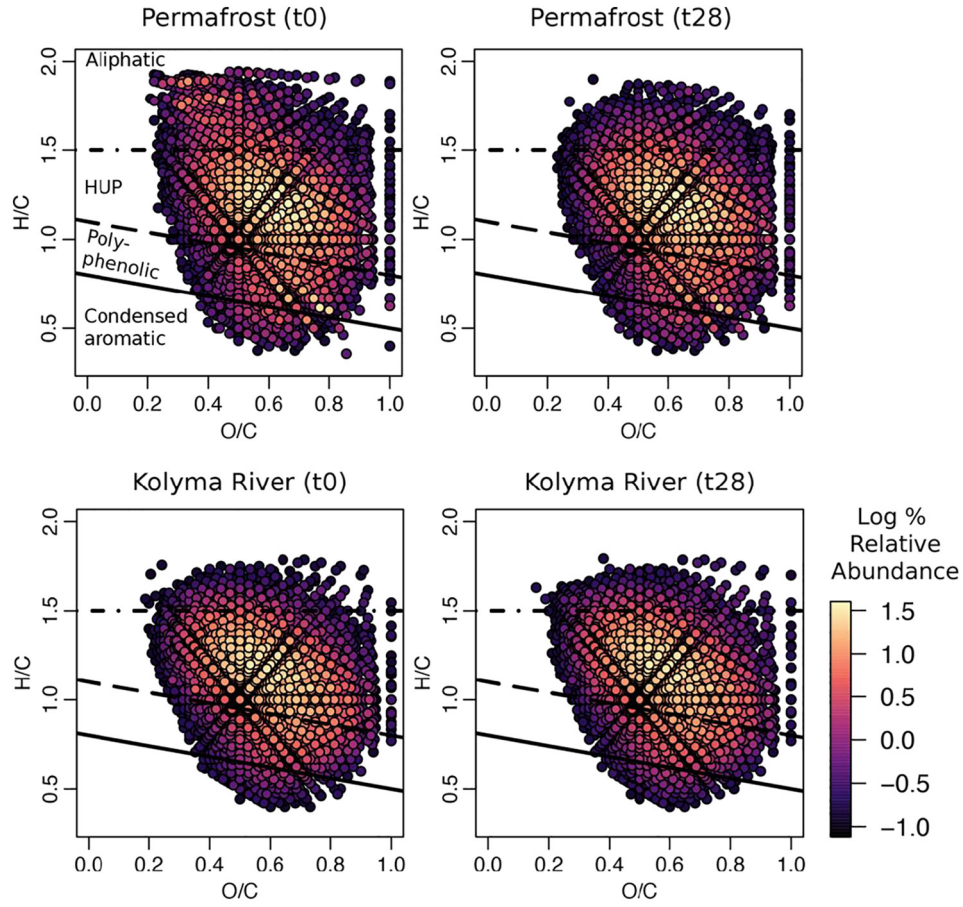


**Figure 2.** Molecular composition of dissolved organic matter (DOM) from the Kolyma River and permafrost water before (t0) and after (t28) incubation as van Krevelen diagrams. Each dot represents a unique DOM molecular formula. Molecular formula is plotted in order of increasing relative abundance, presented as a color gradient on a log scale. Lines associated with specific ratios represent splits among a few of the overarching functional compound classes within the data. The classes presented here are organized vertically from top to bottom as follows: aliphatic, HUP, polyphenolic, and condensed aromatic. The classes are maintained throughout the panels.

and Table 1). This high aliphatic signature and subsequent decrease coincided with the average modified aromaticity index ($AI_{mod}$) value of the sample increasing slightly from 0.293 to 0.296 and the average mass value increasing from 430.6 to 449.6 (Table 1). In the Kolyma River DOM bioincubation, the largest change was a slight decrease in the percent relative abundance of high O/C HUP compounds from 60.7% to 59.5% (Table 1). $AI_{mod}$ for the Kolyma River remained identical and relatively high throughout the incubation process at 0.313 (Table 1).

### 3.2. RPO Thermostability

The thermograms of all samples take a similar form, beginning with a progressive increase in $CO_2$ leading to a distinct dominant peak and finally an abrupt end of the reaction at baseline (Figure 3). The temperature at which the maximum $CO_2$ release occurs ($T_{max}$) varies between 446°C and 499°C, increasing in the following order: permafrost (t0), Kolyma River (t28), Kolyma River (t0), permafrost (t28) (Figure 3). Both of the thermograms for the permafrost DOC present a dampened main peak in comparison to the Kolyma River thermograms and have more $CO_2$ produced at less specific and more broadly distributed temperatures (Figure 3). All samples returned to baseline by 550°C (Figure 3).

After thermograms were transformed into $E$ distributions, the order of main peaks remained the same. Now quantitatively comparable, permafrost DOC at the maximum peak (largest value of $p[0,E]$) shifted during

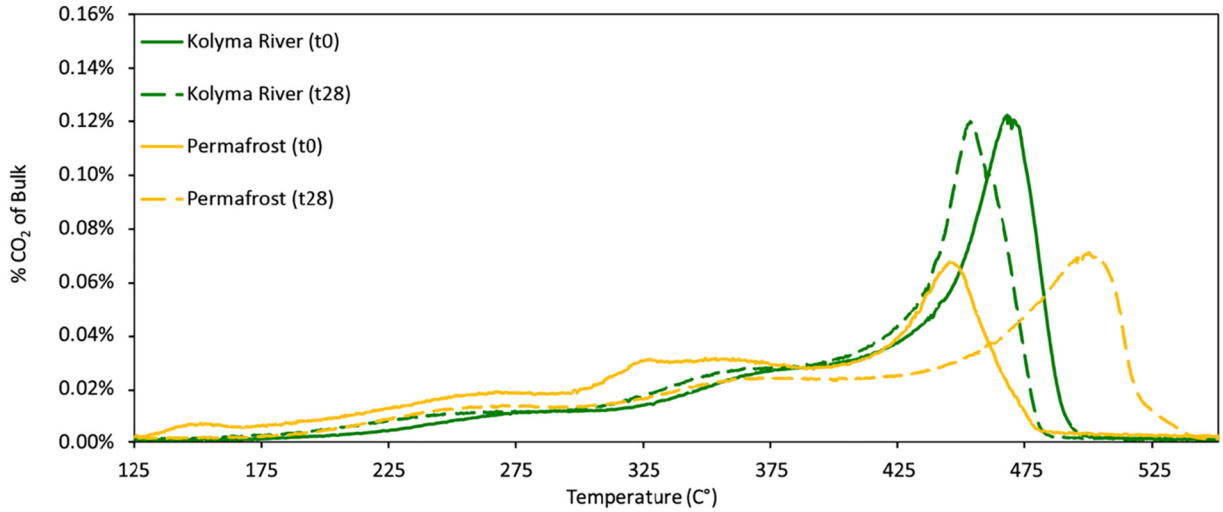


**Figure 3.** Thermograms with the normalized $\%CO_2$ produced as a function of temperature. Dashed lines represent the post-biodegradation samples.

bioincubation from 170 (t0) to 182 (t28) kJ $mol^{-1}$ (Figure 4 and Table 2). In the Kolyma River DOC, *E* distributions remained very similar during bioincubation, with a small decrease in the *E* value of the main peak from 175 (t0) to 172 (t28) kJ $mol^{-1}$ (Figure 5 and Table 2).

### 3.3. RPO $\delta^{13}C$ and $\Delta^{14}C$ Analyses

The bulk $\delta^{13}C$-DOC signature of yedoma thaw stream DOC, with $\delta^{13}C$-DOC values of −26.0‰, has previously been shown to become more depleted following a 28-day bioincubation (Mann et al., 2015). Comparatively, our permafrost DOC fraction values were systematically more depleted with $\delta^{13}C$-DOC averaging −28.8‰ and becoming slightly more enriched after bioincubation (−27.3‰) (Table 3). The Kolyma River saw minimal changes in its $\delta^{13}C$-DOC value during bioincubation (Figure 5 and Table 3). Our Kolyma River (t0) $\delta^{13}C$-DOC at −28.2‰ coincided well with the previously published average value of −28.1‰ (Mann et al., 2015). All of the samples except the permafrost (t28) shared a general trend of becoming more 13C enriched at higher *E* (Table 3). Using a mass balance approach to derive the missing $\delta^{13}C$-DOC value for degraded permafrost DOC (t28) may have contributed to the sample not becoming more 13C enriched at higher *E*. This calculated value was the most enriched, and removing it allows for a linear trend of 13C enrichment coinciding with the remaining samples (Figure 4d). Despite this, the value does not impede further analyses as 13C was not used to model permafrost input.

Permafrost (t0) and (t28) $^{14}C$ fraction Fm values were uniformly low throughout, with no fraction younger than 20,000 $^{14}C$ yBP (Figure 4 and Table 3). The weighted average Fm values showed that relatively younger material was preferentially utilized by microbes resulting in a minor increase in bulk permafrost DOC age from Fm of 0.064, or 22,081 yBP to 0.040, or 25,857 yBP from (t0) to (t28) (Table 3). In the Kolyma River, on the other hand, the DOC was predominantly modern with the lowest Fm fraction value at 0.935, equivalent to 543 $^{14}C$ yBP (Figure 5 and Table 3). Change in post-biodegradation weighted average Fm values for the Kolyma River from (t0) to (t28) was within error (Figure 5 and Table 3).

## 4. Discussion

### 4.1. Assessing DOM Chemical Composition

Through the use of FT-ICR MS, we saw a large number of the aliphatic compounds present in the undegraded permafrost (t0) but absent in the Kolyma River (t0) (Figure S1). Recent studies have noted the relative enrichment of aliphatic assigned formula in yedoma permafrost derived DOM (Drake et al., 2018; MacDonald et al., 2021; Spencer et al., 2015). This aliphatic rich signature (high H/C) is a distinctive characteristic of permafrost-influenced waters and is not reported in either the mainstem of Arctic rivers or other riverine

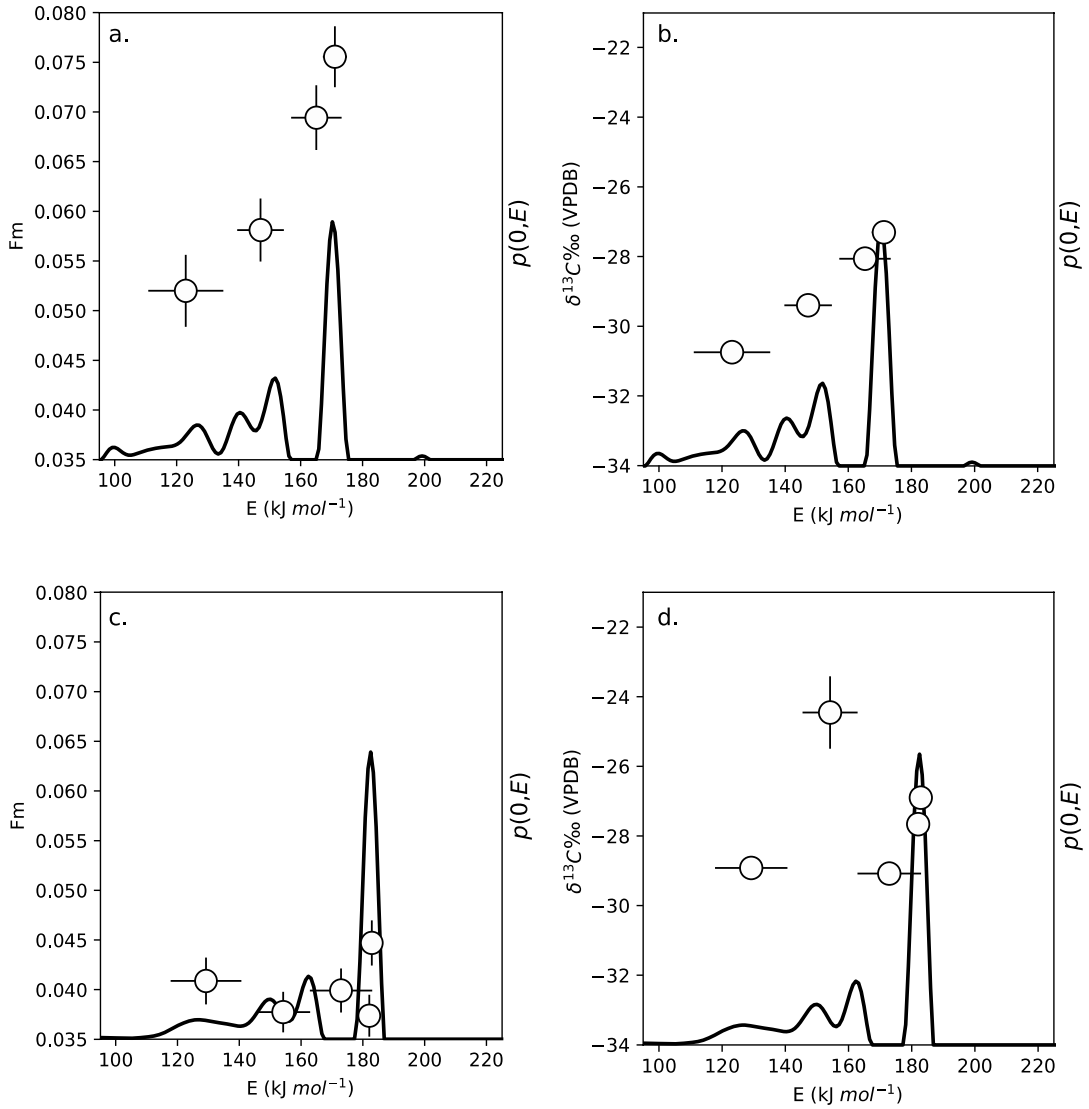


**Figure 4.** Probability density functions of E for permafrost before and after biodegradation. (a) and (b) represent undegraded permafrost (t0), while (c) and (d) represent biodegraded permafrost (t28). In (a) and (c), circles represent the Fm values for each thermal fraction. In (b) and (d), circles represent the $\delta^{13}$C-DOC values for each thermal fraction. The vertical error bars represent the measurement uncertainty and the horizontal error bars represent the standard deviation of the distribution of E within each fraction. Note that axes for Fm between Kolyma River and permafrost vary in values and range length. $p(0,E)$ are proportion values, and the axes remain consistent between panels, and thus they are not presented.

DOM (Drake et al., 2018; Spencer et al., 2015; Stubbins et al., 2010). Put simply, if undegraded permafrost (t0) DOM were to be present in large amounts, this aliphatic signature should be present in the Kolyma River (t0) sample (Figure S1) (Drake et al., 2018; Spencer et al., 2015), and strikingly, it is not.

Permafrost and Kolyma River DOM maintained 73.3% and 83.0% of their formula after bioincubation, respectively (Figure S1). The undegraded permafrost (t0) unique aliphatic formula show the largest reduction in van Krevelen space (Figure S1) during the bioincubation. Other studies have also seen a large decrease in aliphatic compounds in permafrost DOM bioincubations, where aliphatic compounds were positively correlated with BDOC (Spencer et al., 2015; Textor et al., 2019). The relative abundance of HUP high O/C compounds has also been noted to increase post-biodegradation in permafrost DOM (Textor et al., 2019). This emphasizes the difficulty of detecting this unique molecular signature through application of FT-ICR MS in Arctic fluvial networks to identify permafrost inputs as has been noted previously (Spencer et al., 2015).

**Table 2**
*Thermogram and E Distribution Values*

| Sample | Incubation period (Days) | $T_{max}$ (K) | $E_{max}$ (kJ mol$^{-1}$) | $E_{mean}$ (kJ mol$^{-1}$) | $E_{std}$ (kJ mol$^{-1}$) | $p$(0,E) max |
|---|---|---|---|---|---|---|
| Kolyma River | 0 | 740.99 | 175.44 | 165.29 | 16.55 | 0.149 |
| Kolyma River | 28 | 725.14 | 171.93 | 161.20 | 17.85 | 0.155 |
| Permafrost | 0 | 719.01 | 170.18 | 151.77 | 21.46 | 0.085 |
| Permafrost | 28 | 772.12 | 182.46 | 164.50 | 22.73 | 0.103 |

*Note*. Here, $T_{max}$ and $E_{max}$ represent the values at which the largest amount of $CO_2$ was generated. $E_{mean}$ is the weighted mean, taking into account all $CO_2$ generated. $p$(0,$E$) max is the proportion of $CO_2$ associated with the initial $E$ value given for $E_{max}$.

We used the molecular formula presence data to propose that because of conservative mixing there is possibly no undegraded permafrost (t0) in the Kolyma River, however because of the compositional changes following degradation, permafrost that has degraded with time (t28) could be present in larger amounts.

### 4.2. Examining Trends in RPO Thermostability

Notably, the changes in $E$ distribution for permafrost DOC during bioincubation follow the same pattern as the relative loss of aliphatic compounds shown by FT-ICR MS and similarly, for Kolyma River DOC, the minimal change in $E$ distribution mirrors a minimal change in molecular composition (Tables 1 and 2). Among DOC samples previously analyzed on RPO for thermostability ($n$ = 6) (Hemingway et al., 2019), degraded permafrost (t28) was most comparable to a sample from the Pacific Ocean. The Pacific Ocean sample shares a similar $E_{max}$ (182 kJ mol$^{-1}$) and distribution (mean ± s.d.: 166 ± 19 kJ mol$^{-1}$). Of the DOC samples reported to-date ($n$ = 10), these two (our degraded permafrost (t28) and Pacific Ocean) have the highest $E_{max}$. While outside the scope of this study, this may support a phenomenon described in previous studies of degraded terrestrial DOM converging into a signature that is, similar to that of marine DOM (Dittmar et al., 2007; Kellerman et al., 2015; Rossel et al., 2013; Stubbins et al., 2010). All DOC samples ($n$ = 10) returned to baseline around 200 kJ mol$^{-1}$, lower than values reported for other forms of OC (Figure 5) (Hemingway et al., 2019). For example, particulate organic carbon (POC) and sediment organic carbon (SOC) return to baseline at around 250 kJ mol$^{-1}$ (Hemingway et al., 2019). This indicates differences among the properties of these various forms of carbon.

### 4.3. Analyzing Trends Among RPO $\Delta^{14}$C Fractions

For the RPO radiocarbon data, because the oldest fraction within the Kolyma River age structure was only 543 $^{14}$C yBP, none of the Kolyma River (t0) and (t28) fractions was old enough to irrefutably indicate the presence of permafrost DOC (i.e., there does not appear to be a fraction containing highly aged DOC hidden by a dominant modern DOC signal), as was hypothesized (Figure 5 and Table 3). For all sets of fractions, aside from degraded permafrost (t28), which showed no clear trend, there was a minor enrichment in $^{14}$C along the $E$ spectrum (Figures 4 and 5; Table 3). This trend was most pronounced in the undegraded Kolyma River (t0), which had the largest Fm range in our data set, becoming younger at higher $E$, a trend that would be consistent with the presence of highly aliphatic permafrost (Figure 5 and Table 3). This relationship is the inverse of that found for POC and SOC that typically increase in age with increased $E$ and temperature (Grant et al., 2019; Hemingway et al., 2019; Rosenheim & Galy, 2012; Williams et al., 2015). Despite this deviation in trend in relation to other forms of OC, the trend of DOC becoming more modern, or exhibiting no relationship with $E$, has previously been identified in global riverine (e.g., Amazon River) and marine DOC (Hemingway et al., 2019). These observations suggest that slightly depleted $^{14}$C composition at low $E$ in DOC (i.e., thermally labile DOC) is also not clear evidence of permafrost influence. As an aside, this adds further support to the idea that DOC can be aged but relatively more biolabile than more modern DOC (e.g., Guillemette et al., 2017).

### 4.4. Assessment of the Biodegraded Permafrost Component

Overlain plots of DOC $E$ distributions show a distinct lack of overlap in peaks of Kolyma River (t0) to permafrost (t28) DOC (Figure 6a). From here on, Kolyma River (t0) is used instead of (t28) for further assessment of permafrost influence as Kolyma River (t0) differed negligibly from Kolyma River (t28). Instead of converging, as was hypothesized, permafrost derived DOC had a composition after bioincubation that shifted to a higher $E$, past that of the Kolyma River (t0). As biodegraded permafrost (t28) DOC exhibits peaks that are not present in the Kolyma River (t0), its potential contribution to the DOC pool is limited. This conclusion is supported by the premise that $E$ distributions mix conservatively (Hemingway et al., 2018). For example, if one component characterized by high $E$ is mixed with a component characterized by low $E$, the

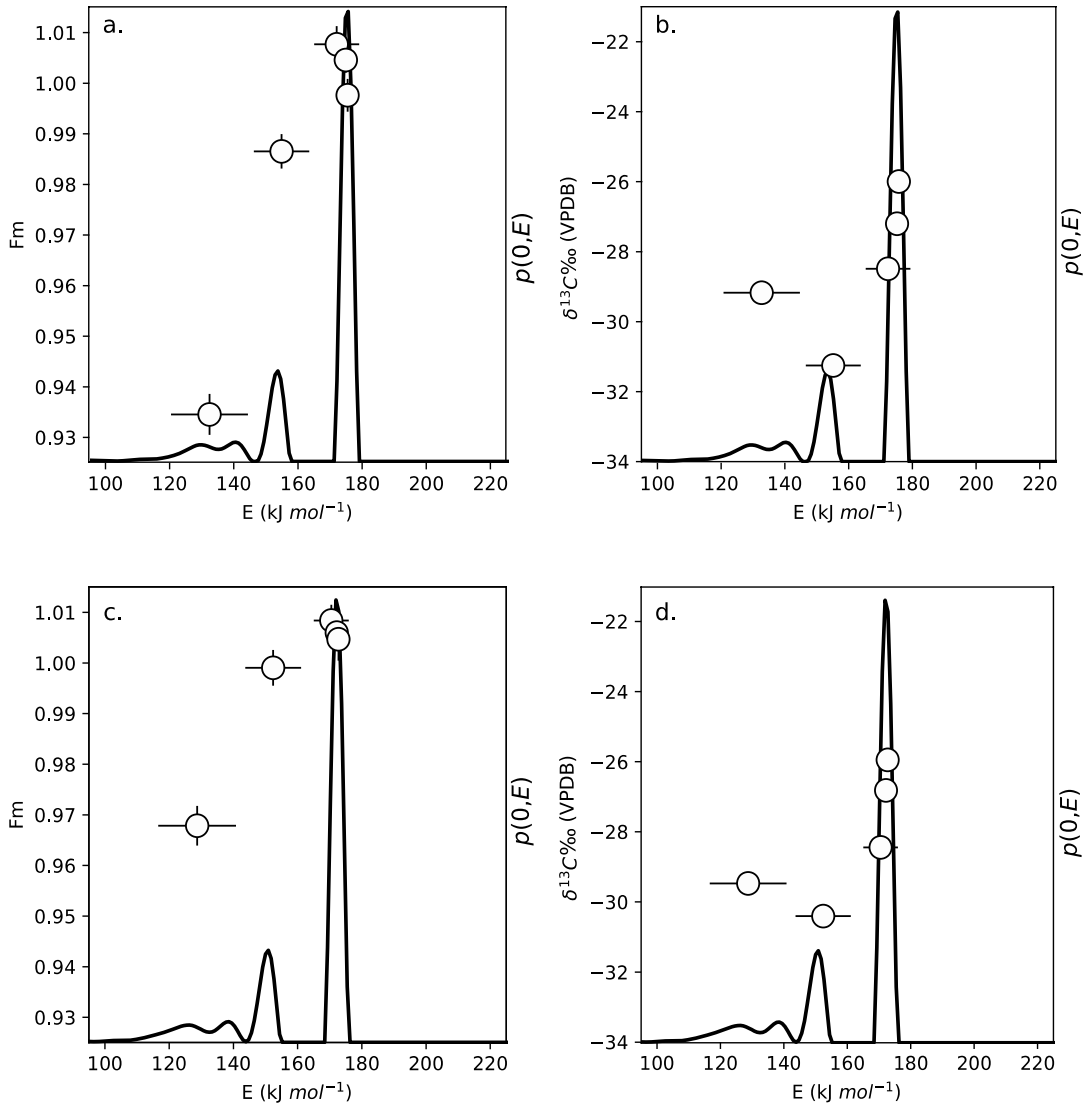


**Figure 5.** Probability density functions of E for the Kolyma River before and after biodegradation. (a) and (b) represent Kolyma River (t0), while c-d represent Kolyma River (t28). In (a) and (c), circles represent the Fm values for each thermal fraction. In (b) and (d), circles represent the $\delta^{13}$C-DOC values for each thermal fraction. The vertical error bars represent the measurement uncertainty, and the horizontal error bars represent the standard deviation of the distribution of $E$ within each fraction. $p(0,E)$ are proportion values, and the axes remain consistent between panels, and thus they are not presented.

resulting $E$ distribution will be of two distinct peaks not a peak centered at an average $E$ value (Hemingway, Rothman et al., 2017, 2018). Of particular importance is the lack of overlap in the maximum peaks as they contain the highest $p(0,E)$, or the highest proportion of carbon associated with a unique set of activation energies; as much as 15.5% for one value (Figure 6a and Table 2).

Because of these shifts, new peaks were formed during permafrost DOC biodegradation that do not overlap with undegraded permafrost (t0), which were distinct even after normalization to DOC loss, verifying their validity as biodegradation products and not simply material which remained after the consumption of biolabile peaks (Figure 6a). These biodegradation products are of distinctly higher $E$ in comparison to the Kolyma River (t0) (Figure 6a). In the Kolyma River (t0), the low temperature fraction, low $E$, has the most $^{14}$C depleted value (Fm = 0.935) with increasing Fm values in consecutive fractions (Figure 5 and Table 3). The production of $^{14}$C depleted DOC formed at high $E$ in permafrost (t28), contrasted with that progressively $^{14}$C

**Table 3**
*The $\delta^{13}$C-DOC and Fm (Age-Corrected $\Delta^{14}$C-DOC) Values for Each Thermally Isolated Fraction and the Amount of Carbon That was Trapped*

| Sample | Incubation period (Days) | Fraction | $\delta^{13}$C (1$\sigma$) | Fm (1$\sigma$) | C Trapped (μg C) |
|---|---|---|---|---|---|
| Kolyma River | 0 | 1 | −29.2 (0.2) | 0.935 (0.004) | 67 |
| Kolyma River | 0 | 2 | −31.3 (0.2) | 0.987 (0.003) | 79 |
| Kolyma River | 0 | 3 | −28.5 (0.2) | 1.008 (0.004) | 88 |
| Kolyma River | 0 | 4 | −27.2 (0.2) | 1.005 (0.003) | 127 |
| Kolyma River | 0 | 5 | −26.0 (0.2) | 0.998 (0.003) | 100 |
| Kolyma River | 0 | Wt. avg. | −28.2 (0.6) | 0.990 (0.023) | 461 |
| Kolyma River | 28 | 1 | −29.5 (0.2) | 0.968 (0.004) | 64 |
| Kolyma River | 28 | 2 | −30.4 (0.2) | 0.999 (0.004) | 76 |
| Kolyma River | 28 | 3 | −28.4 (0.2) | 1.008 (0.003) | 86 |
| Kolyma River | 28 | 4 | −26.8 (0.2) | 1.006 (0.003) | 93 |
| Kolyma River | 28 | 5 | −26.0 (0.2) | 1.005 (0.004) | 78 |
| Kolyma River | 28 | Wt. avg. | −28.1 (0.6) | 0.999 (0.023) | 397 |
| Permafrost | 0 | 1 | −30.8 (0.2) | 0.052 (0.004) | 44 |
| Permafrost | 0 | 2 | −29.4 (0.2) | 0.058 (0.003) | 46 |
| Permafrost | 0 | 3 | −28.1 (0.2) | 0.069 (0.003) | 45 |
| Permafrost | 0 | 4 | −27.3 (0.2) | 0.076 (0.003) | 54 |
| Permafrost | 0 | Wt. avg. | −28.8 (0.7) | 0.064 (0.002) | 189 |
| Permafrost | 28 | 1 | −28.9 (0.3) | 0.041 (0.002) | 78.4 |
| Permafrost | 28 | 2 | −24.5 (1.0)[a] | 0.038 (0.002) | 90.9 |
| Permafrost | 28 | 3 | −29.1 (0.3) | 0.040 (0.002) | 78.4 |
| Permafrost | 28 | 4 | −27.7 (0.3) | 0.037 (0.002) | 97.5 |
| Permafrost | 28 | 5 | −26.9 (0.3) | 0.045 (0.002) | 82.4 |
| Permafrost | 28 | Wt. avg. | −27.3 (0.7) | 0.040 (0.001) | 427.6 |

*Note*. The standard deviation is the measurement uncertainty, propagated with kinetic fractionation and blank correction uncertainty. Wt. avg. is the weighted average of the sum of fractions for a sample, where the standard deviation was propagated and the C trapped is the sum of all fractions.
[a]denotes values that were back calculated from the bulk.

enriched signature at higher *E* in the Kolyma River (t0), continues to suggest no evidence of these permafrost degradation products in the Kolyma River (t0).

### 4.5. Quantification of Permafrost Contribution to the Kolyma River

Overall, our RPO data suggests a lack of biodegraded permafrost DOC (t28) (Section 4.4) in the Kolyma River DOC. However, a broadened overlap between Kolyma River DOC (t0) and permafrost DOC (t0) *E* distribution indicates a possibility for a small fraction of undegraded permafrost DOC (t0) in the Kolyma River (Figure 6b). Thus, we developed a mixing model based on *E* distributions and radiocarbon composition to estimate the quantity of undegraded permafrost (t0) in the Kolyma River (t0). Because we lack continuous $^{14}$C data across the *E* distribution, the mixing model needs to be discretized. We split the *E* distributions at 160 kJ mol$^{-1}$, as there is no OC associated with that *E* value. The relative contribution of the two splits to the total area was 53.8% and 46.2% for permafrost (t0) and 30.5% and 69.5% for the Kolyma River (t0), below and above 160 kJ mol$^{-1}$, respectively. The ages were also split resulting in Fm values of 0.0551 and 0.0728 for permafrost (t0) and 0.9622 and 1.0032 for the Kolyma River (t0). Input from a modern endmember is used to account for the area within the Kolyma River area minus the permafrost area (each scaled by the estimated percent contribution) to build a mixing model. Conceptually, we tested how much undegraded permafrost

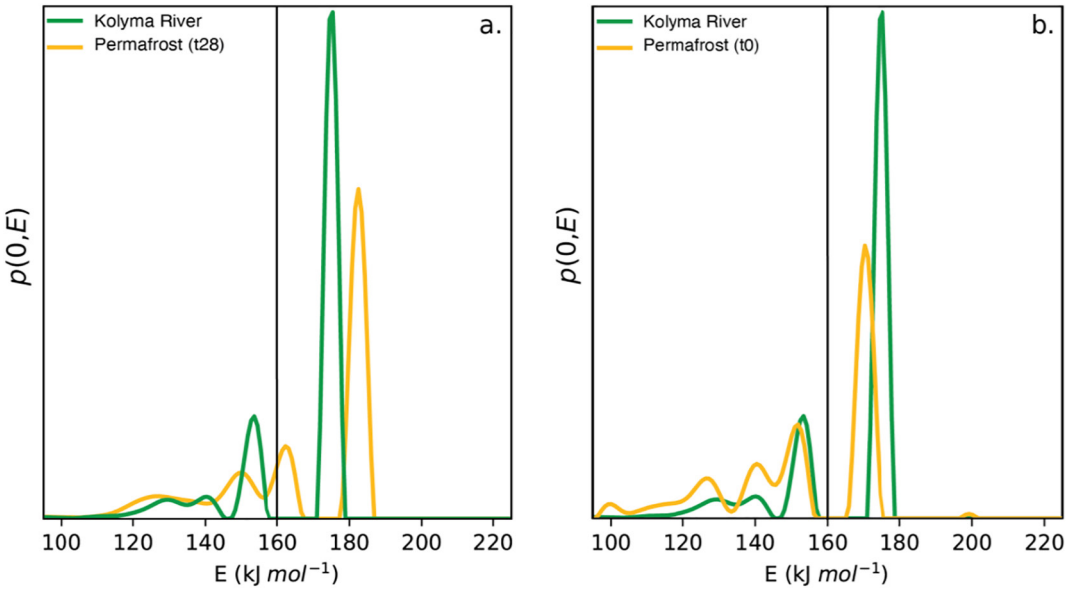


**Figure 6.** The overlain E distributions for justification of a proportion mixing model. (a) the Kolyma River (t0) and degraded permafrost (t28) and (b) the Kolyma River (t0) and undegraded permafrost (t0). The line represents a split in the E space at 160 kJ mol$^{-1}$.

(t0) DOC can be mixed with a chosen "modern" DOC endmember before reaching a $^{14}$C age (above and below 160 kJ mol$^{-1}$) that is, compatible with the observed Kolyma River DOC (Figure 7).

$$\%\text{permafrost} = \left( \frac{A_{KR} \times \left( Fm_{modern} - Fm_{KR} \right)}{A_{perm} \times \left( Fm_{modern} - Fm_{perm} \right)} \right) * 100 \quad (1)$$

Here, $Fm_{perm}$, $Fm_{KR}$, and $Fm_{modern}$ represent the radiocarbon values for the permafrost (t0), the Kolyma River (t0), and the modern endmember, respectively; and $A_{perm}$ and $A_{KR}$ denote the percent of the area for the permafrost (t0) and the Kolyma River, respectively. Equation 1 was used to calculate the maximum permafrost contribution to each split (above and below 160 kJ mol$^{-1}$). The final % permafrost contribution is the smaller of the two as one side of the thermogram cannot be older than that observed in the Kolyma River ($Fm_{KR}$) while the two splits cannot receive different amounts of permafrost input. Consequently, an additional input from a moderately aged DOC endmember (e.g., active layer input) may be required to account for the offset once one split reaches the threshold for permafrost input. Percent permafrost contribution was solved three times using different modern terrestrial endmembers, as each offer a different perspective on the underlying age of Kolyma River DOC. Evaluating the three modern terrestrial endmembers allows us to develop as robust an estimate of permafrost contribution to the Kolyma River as possible. Error was propagated through the mixing model using Kolyma River (t0) and permafrost (t0) Fm measurement uncertainties, as well as either the uncertainties or the standard deviation of the three modern endmembers.

We used the most modern Kolyma River DOC fraction from this study as the first modern endmember representing contemporary riverine DOC (Fm = 0.935 ± 0.004; $n$ = 1), with the assumption that our most modern fraction contains no permafrost C. This yields a maximum permafrost contribution of 0.84 ± 3.26% (Figure 7a). This value closely matches an estimate of 0.7 ± 0.1% permafrost derived DOC in the Kolyma River mainstem, for which a Bayesian mixing model approach was implemented using Monte Carlo simulations (Mann et al., 2015).

A second terrestrial modern endmember was generated from literature values ($n$ = 58), which represents the litter and organic layer of the pan-Arctic (Wild et al., 2019). Using this value (Fm = 1.104 ± 0.13), our mixing model yields a maximum permafrost DOC contribution of 7.68% ± 5.89% (Figure 7b). Comparatively, a previous estimate of permafrost contribution to Kolyma River DOC in "summer/fall" using the same modern endmember corresponded to 7.3 ± 2.9%, based on a Monte Carlo approach (Wild et al., 2019).

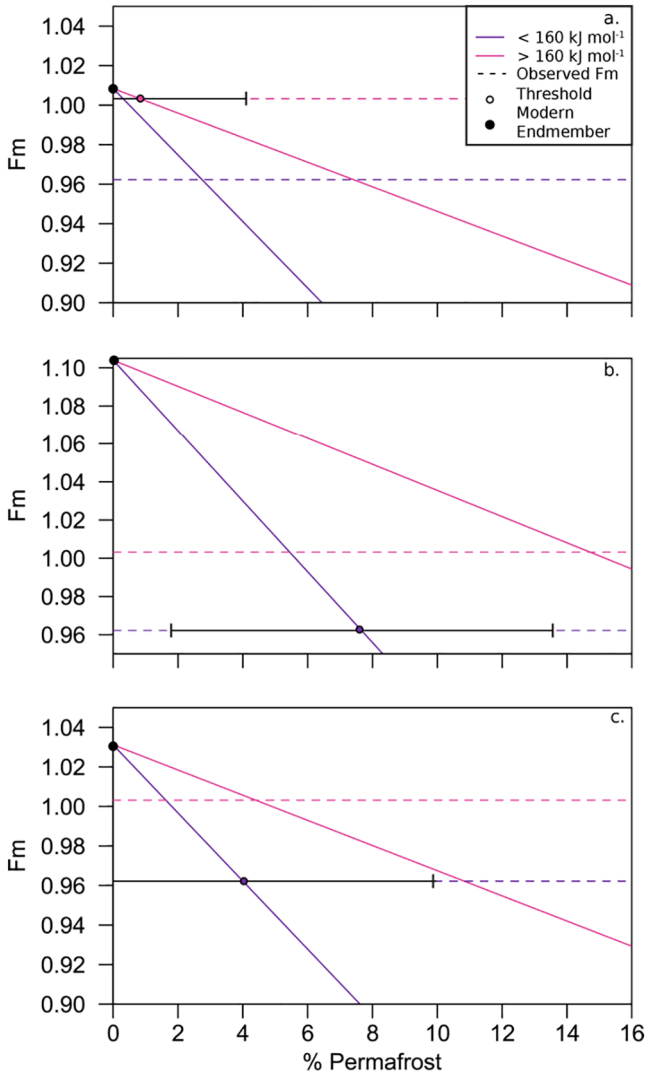


**Figure 7.** Maximum percent permafrost contribution to Kolyma River dissolved organic carbon (DOC) based on an end-member mixing model using three modern terrestrial DOC Fm endmember values. Black filled circles on the *y*-axis represent Fm values of three modern endmembers derived from (a) the most modern Kolyma River value from this study, (b) Arctic litter and organic layers (Wild et al., 2019), and (c) global riverine DOC (Marwick et al., (2015)). The maximum amount of % permafrost contribution is the lower of the two % permafrost values reached when the mixing line (solid) reaches its corresponding dotted line of the same color. When the mixing line (solid) crosses its coinciding dotted line of the same color is when permafrost inputs cause the *E* distribution to be older than observed. Error bars represent propagated standard deviation. Note that the *y*-axis varies per panel.

This value represented their "minimum scenario," which used a permafrost endmember comprising only Pleistocene aged permafrost (i.e., $\Delta^{14}$C-DOC = −955 ± 66‰ equal to 24,800 yBP) and was similar to our estimate because we also used a Pleistocene aged permafrost DOC endmember at 23,963 yBP.

Finally, we used global riverine $\Delta^{14}$C-DOC values as a modern endmember (Marwick et al., 2015). All Arctic samples were conservatively removed due to the potential for permafrost contributions. Collection dates were assumed as measurement dates when converting to Fm ($n$ = 506). This endmember value (Fm = 1.031 ± 0.110) yielded a maximum % permafrost contribution of 4.00 ± 5.95 (Figure 7c). This value is conservative in that global riverine DOC has aged components at lower *E* unrelated to permafrost contributions (Section 4.3) (Hemingway et al., 2019).

The use of three discrete modern terrestrial endmembers constrains maximum permafrost inputs for the Kolyma River between ~0.8% and 8% of riverine DOC in late summer (i.e., the period of maximum permafrost thaw). Clearly, the estimate of a reasonable "modern" endmember alters the maximum contribution of permafrost; however, the contribution remains relatively small. Additionally, whether undegraded (t0) or degraded (t28) permafrost was chosen to represent the primary source of aged material in the mixing model, both would result in a similar estimate of contribution, since both permafrost (t0) and (t28) are of similar age.

In reference to the lack of thermochemical convergence between permafrost (t28) and the Kolyma River (t0), we propose a few mechanisms worthy of investigation. In particular, the impacts of photo-oxidation and sorption on DOC RPO thermostability have yet to be assessed, and these processes may shift *E* distribution. In some Arctic regions, the role of photochemistry in streams has been shown to be an important pathway for degradation of permafrost DOM (Bowen et al., 2020; Ward & Cory, 2016). Of relevance to this study, photo-oxidation selectively reduces aromaticity in the DOM pool while relatively increasing aliphatic and oxygen-containing compounds (Stubbins et al., 2010; Ward & Cory, 2016). This could lead to a shift to lower *E*. Yedoma DOM is not susceptible to photo-mineralization into $CO_2$; however, photo-modification of permafrost could potentially play a role in shifting the *E* distribution (Cory et al., 2013; Stubbins et al., 2017). This could help explain the lack of convergence in biodegraded permafrost (t28) *E* to that of the Kolyma River (t0), if photochemical reactions were to significantly influence permafrost DOM. The controlling processes in Arctic streams remains an area of ongoing debate (Cory & Kling, 2018; Cory et al., 2013; Rocher-Ros et al., 2020); however, no FT-ICR MS compositional parameter increased or decreased for degraded permafrost beyond that of the Kolyma River to account for the overall shift to higher *E* post-degradation, obscuring insight into the possible effects of photo-modification in our data set (Table 1). Future studies will be necessary to determine the effects of photochemistry on thermostability as no literature currently documents these effects.

Another mechanism that could explain the lack of convergence between permafrost (t28) and Kolyma River (t0) is colloidal aggregation. Colloidal aggregation affects the apparent bond-strength of DOC, that is, thermostability, and is particularly relevant in samples with high iron concentrations (Simpson et al., 2002). Permafrost thaw has been previously cited to liberate iron into Siberian rivers at concentrations two to five times the global average (Pokrovsky et al., 2006). The effects of iron release could be two-fold. First, it may cause a broader *E* distribution by increasing bond-strength diversity (Hemingway et al., 2019), as

in permafrost (t0) and (t28) (Figure 4). Second, it could cause low *E* compounds to aggregate and thus be protected from *in situ* biodegradation (Barber et al., 2017; Hemingway et al., 2019), perhaps explaining the occurrence of $^{14}$C-depletion at low *E* values that is, seen in our samples (Figures 4 and 5). The effect of iron on thermostability was suggested for POC and SOC (Barber et al., 2017; Hemingway et al., 2019), and less is known about its effect on the overall depiction and interpretation of DOC thermostability. Finally, the inverse age trend and the *E* distribution of samples (e.g., the location of the maximum peak for permafrost [t0]), may be an artifact of the combustion process, where RPO has the potential to char biolabile, young components to appear more refractory. While the potential for char production during RPO has only been assessed for SOC (Williams et al., 2014) and potential char production did not impact previous assessments (Hemingway et al., 2019), char is unlikely in our study as the charred material would be expected at higher *E* values than what was observed.

### 4.6. Implications for Permafrost DOM Influence

By 2300, Arctic surface air temperatures are expected to rise by around 3–13°C (McGuire et al., 2018). Without proper mitigation, this will lead to extensive permafrost thaw and the release of carbon as greenhouse gases, with a mean estimate of 341 Pg C (McGuire et al., 2018). The mobilization of a large amount of permafrost organic matter into fluvial ecosystems as DOM is also expected (Vonk & Gustafsson, 2013). Current estimates of permafrost DOM mobilization into fluvial networks are not yet clear due to several constraints, particularly the lack of a specific tracer for aged permafrost inputs (i.e., the radiocarbon age of bulk DOC is a mean age that might mask permafrost contributions). Regardless, it is important to establish a robust understanding of permafrost DOM currently integrating into Arctic river systems and chemical processes governing alterations to better predict future changes. Soils in the Kolyma River catchment consist entirely of continuous permafrost with large swaths of organic matter rich yedoma (Anthony et al., 2014; Holmes et al., 2012; Strauss et al., 2013), yet bulk carbon isotopic analyses highlight the predominantly modern signature of Kolyma River DOC (Drake et al., 2018; Mann et al., 2015; Spencer et al., 2015; Wild et al., 2019).

This study utilized an innovative mechanistic approach combining ultrahigh-resolution mass spectrometry and age structure analyses viewed under the lens of thermostability. First, we did not observe a hidden, distinctly permafrost-age component in the Kolyma River as the oldest value represented ~500 $^{14}$C yBP. Second, permafrost (t0) was observed to have a distinct molecular signature that is, not present in the Kolyma River, which suggests minimal addition of undegraded permafrost (t0) to the Kolyma River (Figure S1) (Drake et al., 2018; Spencer et al., 2015). Though we found biodegradation to obscure source contributions for our molecular composition data, a lack of thermochemical convergence for biodegraded permafrost (t28) using RPO instead offered clarity. RPO suggested minimal inputs of degraded permafrost with the formation of degradation products at high *E* values though simultaneously offered a means to measure undegraded permafrost contributions. Thermostability then was employed alongside radiocarbon composition allowing us to deconvolute Kolyma River DOC using an endmember mixing model. The mixing model allowed us to estimate undegraded permafrost (t0) contribution as a maximum 0.8 $\pm$ 3.3% to 7.7 $\pm$ 5.9% of Kolyma River (t0) DOC. Since there appears to be no degraded permafrost (t28) identified in the Kolyma River mainstem at Cherskiy, the maximum input value may in fact represent the total DOC concentration of permafrost thaw at the source to the Kolyma River at the time of maximum thaw depth and permafrost input in late summer. While these values may appear small, they translate to an annual permafrost DOC flux of 0.05 Tg C y$^{-1}$ of the 0.82 Tg C y$^{-1}$ the Kolyma River exports to the Arctic Ocean (Wild et al., 2019). The Kolyma watershed's larch forests (assuming the same sequestration rates as the Lena watershed) sequester on average 575 Mg of C daily from July to October, a rate dampened by the annual shift from sink to source (Dolman et al., 2004; Holmes et al., 2012). Meanwhile, at its peak we maintain that the Kolyma River could reach a daily longitudinal permafrost DOC flux of 206 Mg, releasing close to half the sequestering amount into the river to be respired (Holmes et al., 2012). This represents an OC source that was formerly inaccessible and is preferentially utilized by microbes, potentially adding to global greenhouse gas emissions (Drake et al., 2015, 2018; Mann et al., 2015; Vonk et al., 2013).

Based on these findings, FT-ICR MS qualitatively excluded the possibility of large quantities of undegraded permafrost (t0) input to the Kolyma River and RPO excluded the possibility of large quantities of degraded permafrost input (t28). Our RPO $^{14}$C-DOC data reveal that moderately old DOC inputs may be responsible

for Kolyma River DOC ages (see Fm values for Kolyma River Fraction 1, Figure 5 and Table 3) rather than a higher estimate of ancient permafrost DOC contribution. This conservative approach presents novel insight into the complex nature of endmember mixing and reveals that permafrost export from Arctic rivers may be limited. Our findings imply that modern DOC inputs dominate the signature of the Kolyma River. This study, however, does not preclude *in situ* permafrost pore water remineralization or extensive thaw. Active layer deepening and degradation of permafrost soils and associated pore water could in fact represent a more dominant form of OC loss given its high bioavailability (Åkerman & Johansson, 2008; Schuur et al., 2015; Vasiliev et al., 2020; Vonk et al., 2015). The end result being permafrost DOC degrades releasing $CO_2$ from the terrestrial surface to the atmosphere. Future investigations examining permafrost OC utilization will require a multidisciplinary approach crossing the boundary of soil and aqueous biogeochemistry to examine biodegradation at the site of thaw.

## Data Availability Statement

The evolution of $CO_2$ per increasing temperature data which constitute the thermograms and are subsequently used in the inverse modeling can be accessed online using the EarthChem Library (https://doi.org/10.26022/IEDA/111617) (Rogers, Jennifer et al., 2020).

**Acknowledgments**
The authors thank the staff at the Northeast Science Station in Cherskiy for their assistance with field sampling. This work was funded by NSF grants ANT-1203885 and PLR-1500169 to R.G.M.S. The work was also supported by the National Science Foundation Division of Chemistry through DMR-1644779 and the State of Florida. The authors thank all people in the NHMFL ICR Program that work to facilitate data acquisition and processing for users of the facility. Additional thanks to everyone at National Ocean Sciences Accelerator Mass Spectrometry and the Woods Hole Oceanographic Institution for their assistance in radiocarbon analyses. The authors also thank Greg Fiske at the Woods Hole Research Center for making the site map. And a final thanks to Sarah Ellen Johnston for her patient guidance and mentorship.

## References

Abbott, B. W., Jones, J. B., Godsey, S. E., Larouche, J. R., & Bowden, W. B. (2015). Patterns and persistence of hydrologic carbon and nutrient export from collapsing upland permafrost (preprint). *Biogeosciences*, *12*(12), 3725–3740. https://doi.org/10.5194/bgd-12-2063-2015

Abbott, B. W., Larouche, J. R., Jones, J. B., Bowden, W. B., & Balser, A. W. (2014). Elevated dissolved organic carbon biodegradability from thawing and collapsing permafrost. *Journal of Geophysical Research: Biogeosciences*, *119*(10), 2049–2063. https://doi.org/10.1002/2014JG002678

Åkerman, H. J., & Johansson, M. (2008). Thawing permafrost and thicker active layers in sub-arctic Sweden. *Permafrost and Periglacial Processes*, *19*(3), 279–292. https://doi.org/10.1002/ppp.626

Anthony, K. M. W., Zimov, S. A., Grosse, G., Jones, M. C., Anthony, P. M., Iii, F. S. C., et al. (2014). A shift of thermokarst lakes from carbon sources to sinks during the Holocene epoch. *Nature*, *511*(7510), 452–456. https://doi.org/10.1038/nature13560

Barber, A., Brandes, J., Leri, A., Lalonde, K., Balind, K., Wirick, S., et al. (2017). Preservation of organic matter in marine sediments by inner-sphere interactions with reactive iron. *Scientific Reports*, *7*(1), 1–10. https://doi.org/10.1038/s41598-017-00494-0

Blakney, G. T., Hendrickson, C. L., & Marshall, A. G. (2011). Predator data station: A fast data acquisition system for advanced FT-ICR MS experiments. *International Journal of Mass Spectrometry*, *306*(2), 246–252. https://doi.org/10.1016/j.ijms.2011.03.009

Bowen, J. C., Ward, C. P., Kling, G. W., & Cory, R. M. (2020). Arctic amplification of global warming strengthened by sunlight oxidation of permafrost carbon to $CO_2$. *Geophysical Research Letters*, *47*(12), e2020GL087085. https://doi.org/10.1029/2020GL087085

Corilo, Y. E. (n.d.). *PetroOrg software*. Tallahassee, FL: Florida State University.

Cory, R. M., Crump, B. C., Dobkowski, J. A., & Kling, G. W. (2013). Surface exposure to sunlight stimulates $CO_2$ release from permafrost soil carbon in the Arctic. *Proceedings of the National Academy of Sciences*, *110*(9), 3429–3434. https://doi.org/10.1073/pnas.1214104110

Cory, R. M., & Kling, G. W. (2018). Interactions between sunlight and microorganisms influence dissolved organic matter degradation along the aquatic continuum. *Limnology and Oceanography Letters*, *3*(3), 102–116. https://doi.org/10.1002/lol2.10060

D'Andrilli, J., Cooper, W. T., Foreman, C. M., & Marshall, A. G. (2015). An ultrahigh-resolution mass spectrometry index to estimate natural organic matter lability. *Rapid Communications in Mass Spectrometry: Rapid Communications in Mass Spectrometry*, *29*(24), 2385–2401. https://doi.org/10.1002/rcm.7400

De la Rosa, J., Merino, A., Jiménez-Morillo, N., Jiménez-González, M., González-Pérez, J., González-Vila, F. J., et al. (2018). *Unveiling the effects of fire on soil organic matter by spectroscopic and thermal degradation methods*. CRC Press.

De la Rosa, J. M., González-Pérez, J. A., González-Vázquez, R., Knicker, H., López-Capel, E., Manning, D. A. C., & González-Vila, F. J. (2008). Use of pyrolysis/GC-MS combined with thermal analysis to monitor C and N changes in soil organic matter from a Mediterranean fire affected forest. *Catena*, *74*(3), 296–303. https://doi.org/10.1016/j.catena.2008.03.004

Dittmar, T., Koch, B., Hertkorn, N., & Kattner, G. (2008). A simple and efficient method for the solid-phase extraction of dissolved organic matter (SPE-DOM) from seawater. *Limnology and Oceanography: Methods*, *6*(6), 230–235. https://doi.org/10.4319/lom.2008.6.230

Dittmar, T., Whitehead, K., Minor, E. C., & Koch, B. P. (2007). Tracing terrigenous dissolved organic matter and its photochemical decay in the ocean by using liquid chromatography/mass spectrometry. *Marine Chemistry*, *107*(3), 378–387. https://doi.org/10.1016/j.marchem.2007.04.006

Dolman, A. J., Maximov, T. C., Moors, E. J., Maximov, A. P., Elbers, J. A., Kononov, A. V., et al. (2004). Net ecosystem exchange of carbon dioxide and water of far eastern Siberian Larch (Larix cajanderii) on permafrost. *Biogeosciences*, *1*(2), 133–146. https://doi.org/10.5194/bg-1-133-2004

Drake, T., Guillemette, F., Hemingway, J., Chanton, P. J., Podgorski, D., Zimov, S. N., & Spencer, R. (2018). The ephemeral signature of permafrost carbon in an Arctic fluvial network. *Journal of Geophysical Research: Biogeosciences*, *123*(5), 1475–1485. https://doi.org/10.1029/2017JG004311

Drake, T. W., Wickland, K. P., Spencer, R. G. M., McKnight, D. M., & Striegl, R. G. (2015). Ancient low-molecular-weight organic acids in permafrost fuel rapid carbon dioxide production upon thaw. *Proceedings of the National Academy of Sciences*, *112*(45), 13946–13951. https://doi.org/10.1073/pnas.1511705112

Ewing, S. A., O'Donnell, J. A., Aiken, G. R., Butler, K., Butman, D., Windham-Myers, L., & Kanevskiy, M. Z. (2015). Long-term anoxia and release of ancient, labile carbon upon thaw of Pleistocene permafrost. *Geophysical Research Letters*, *42*(24), 730–810. https://doi.org/10.1002/2015GL066296

Grant, K. E., Galy, V. V., Chadwick, O. A., & Derry, L. A. (2019). Thermal oxidation of carbon in organic matter rich volcanic soils: Insights into SOC age differentiation and mineral stabilization. *Biogeochemistry*, *144*(3), 291–304. https://doi.org/10.1007/s10533-019-00586-1

Guillemette, F., Bianchi, T. S., & Spencer, R. G. M. (2017). Old before your time: Ancient carbon incorporation in contemporary aquatic foodwebs. *Limnology & Oceanography*, *62*(4), 1682–1700. https://doi.org/10.1002/lno.10525

Hemingway, J. D. (2018). *FluvialSeds/rampedpyrox*. Python. Retrieved from https://github.com/FluvialSeds/rampedpyrox

Hemingway, J. D., Galy, V. V., Gagnon, A. R., Grant, K. E., Rosengard, S. Z., Soulet, G., et al. (2017). Assessing the blank carbon contribution, isotope mass balance, and kinetic isotope fractionation of the ramped pyrolysis/oxidation instrument at NOSAMS. *Radiocarbon*, *59*(1), 179–193. https://doi.org/10.1017/RDC.2017.3

Hemingway, J. D., Hilton, R. G., Hovius, N., Eglinton, T. I., Haghipour, N., Wacker, L., et al. (2018). Microbial oxidation of lithospheric organic carbon in rapidly eroding tropical mountain soils. *Science*, *360*(6385), 209–212. https://doi.org/10.1126/science.aao6463

Hemingway, J. D., Rothman, D. H., Grant, K. E., Rosengard, S. Z., Eglinton, T. I., Derry, L. A., & Galy, V. V. (2019). Mineral protection regulates long-term global preservation of natural organic carbon. *Nature*, *570*(7760), 228–231. https://doi.org/10.1038/s41586-019-1280-6

Hemingway, J. D., Rothman, D. H., Rosengard, S. Z., & Galy, V. V. (2017). Technical note: An inverse method to relate organic carbon reactivity to isotope composition from serial oxidation. *Biogeosciences*, *14*(22), 5099–5114. https://doi.org/10.5194/bg-14-5099-2017

Hendrickson, C. L., Quinn, J. P., Kaiser, N. K., Smith, D. F., Blakney, G. T., Chen, T., et al. (2015). 21 Tesla Fourier transform ion cyclotron resonance mass spectrometer: A national resource for ultrahigh resolution mass analysis. *Journal of The American Society for Mass Spectrometry*, *26*(9), 1626–1632. https://doi.org/10.1007/s13361-015-1182-2

Holmes, R. M., McClelland, J. W., Peterson, B. J., Tank, S. E., Bulygina, E., Eglinton, T. I., et al. (2012). Seasonal and annual fluxes of nutrients and organic matter from large rivers to the Arctic Ocean and surrounding seas. *Estuaries and Coasts*, *35*(2), 369–382. https://doi.org/10.1007/s12237-011-9386-6

IPCC. (2013). *Climate change 2013. Summary for policymakers*. Cambridge: Cambridge University Press.

Kellerman, A. M., Kothawala, D. N., Dittmar, T., & Tranvik, L. J. (2015). Persistence of dissolved organic matter in lakes related to its molecular characteristics. *Nature Geoscience*, *8*(6), 454–457. https://doi.org/10.1038/ngeo2440

Koch, B. P., & Dittmar, T. (2006). From mass to structure: An aromaticity index for high-resolution mass data of natural organic matter. *Rapid Communications in Mass Spectrometry*, *20*(5), 926–932. https://doi.org/10.1002/rcm.2386

Koch, B. P., & Dittmar, T. (2016). From mass to structure: An aromaticity index for high-resolution mass data of natural organic matter. *Rapid Communications in Mass Spectrometry*, *30*(1), 250. https://doi.org/10.1002/rcm.7433

Kujawinski, E. B. (2002). Electrospray ionization Fourier transform ion cyclotron resonance mass spectrometry (ESI FT-ICR MS): Characterization of complex environmental mixtures. *Environmental Forensics*, *3*(3), 207–216. https://doi.org/10.1006/enfo.2002.0109

Kurek, M. R., Poulin, B. A., McKenna, A. M., & Spencer, R. G. M. (2020). Deciphering dissolved organic matter: Ionization, dopant, and fragmentation insights via Fourier transform-ion cyclotron resonance mass spectrometry. *Environmental Science & Technology*, *54*(24), 16249–16259. https://doi.org/10.1021/acs.est.0c05206

Leifeld, J., & von Lützow, M. (2014). Chemical and microbial activation energies of soil organic matter decomposition. *Biology and Fertility of Soils*, *50*(1), 147–153. https://doi.org/10.1007/s00374-013-0822-6

MacDonald, E. N., Tank, S. E., Kokelj, S. V., Froese, D. G., & Hutchins, R. H. S. (2021). Permafrost-derived dissolved organic matter composition varies across permafrost end-members in the western Canadian Arctic. *Environmental Research Letters*, *16*, 024036. https://doi.org/10.1088/1748-9326/abd971

Mann, P. J., Eglinton, T. I., McIntyre, C. P., Zimov, N., Davydova, A., Vonk, J. E., et al. (2015). Utilization of ancient permafrost carbon in headwaters of Arctic fluvial networks. *Nature Communications*, *6*, 7856. https://doi.org/10.1038/ncomms8856

Marwick, T. R., Tamooh, F., Teodoru, C. R., Borges, A. V., Darchambeau, F., & Bouillon, S. (2015). The age of river-transported carbon: A global perspective. *Global Biogeochemical Cycles*, *29*(2), 122–137. https://doi.org/10.1002/2014GB004911

McGuire, A. D., Lawrence, D. M., Koven, C., Clein, J. S., Burke, E., Chen, G., et al. (2018). Dependence of the evolution of carbon dynamics in the northern permafrost region on the trajectory of climate change. *Proceedings of the National Academy of Sciences*, *115*(15), 3882–3887. https://doi.org/10.1073/pnas.1719903115

O'Donnell, J. A., Aiken, G. R., Butler, K. D., Guillemette, F., Podgorski, D. C., & Spencer, R. G. M. (2016). DOM composition and transformation in boreal forest soils: The effects of temperature and organic-horizon decomposition state. *Journal of Geophysical Research: Biogeosciences*, *121*(10), 2727–2744. https://doi.org/10.1002/2016JG003431

Peltre, C., Fernández, J. M., Craine, J. M., & Plante, A. F. (2013). Relationships between biological and thermal indices of soil organic matter stability differ with soil organic carbon level. *Soil Science Society of America Journal*, *77*(6), 2020–2028. https://doi.org/10.2136/sssaj2013.02.0081

Pokrovsky, O. S., Schott, J., & Dupré, B. (2006). Trace element fractionation and transport in boreal rivers and soil porewaters of permafrost-dominated basaltic terrain in Central Siberia. *Geochimica et Cosmochimica Acta*, *70*(13), 3239–3260. https://doi.org/10.1016/j.gca.2006.04.008

Reimer, P. J., Brown, T. A., & Reimer, R. W. (2004). *Reporting and calibration OF post-BOMB $^{14}C$ data*. Lawrence Livermore National Laboratory.

Rocher-Ros, G., Harms, T., Sponseller, R., Väisänen, M., Mörth, C.-M., & Giesler, R. (2020). Metabolism overrides photo-oxidation in $CO_2$ dynamics of Arctic permafrost streams. *Limnology & Oceanography*, *1*. https://doi.org/10.1002/lno.11564

Rogers, J., Galy, V., Kellerman, A., Chanton, J., Zimov, N., & Spencer, R. (2020). *Ramped temperature CO2 evolution for permafrost and Kolyma River dissolved organic carbon (version 1.0)*. Interdisciplinary Earth Data Alliance (IEDA). https://doi.org/10.26022/IEDA/111617

Rosenheim, B. E., Day, M. B., Domack, E., Schrum, H., Benthien, A., & Hayes, J. M. (2008). Antarctic sediment chronology by programmed-temperature pyrolysis: Methodology and data treatment. *Geochemistry, Geophysics, Geosystems*, *9*(4). Q04005. https://doi.org/10.1029/2007GC001816

Rosenheim, B. E., & Galy, V. (2012). Direct measurement of riverine particulate organic carbon age structure. *Geophysical Research Letters*, *39*(19). L19703. https://doi.org/10.1029/2012GL052883

Rosenheim, B. E., Roe, K. M., Roberts, B. J., Kolker, A. S., Allison, M. A., & Johannesson, K. H. (2013). River discharge influences on particulate organic carbon age structure in the Mississippi/Atchafalaya River System. *Global Biogeochemical Cycles*, *27*(1), 154–166. https://doi.org/10.1002/gbc.20018

Rossel, P. E., Vähätalo, A. V., Witt, M., & Dittmar, T. (2013). Molecular composition of dissolved organic matter from a wetland plant (Juncus effusus) after photochemical and microbial decomposition (1.25 yr): Common features with deep sea dissolved organic matter. *Organic Geochemistry*, *60*, 62–71. https://doi.org/10.1016/j.orggeochem.2013.04.013

Sanderman, J., & Grandy, A. S. (2020). Ramped thermal analysis for isolating biologically meaningful soil organic matter fractions with distinct residence times. *Soil*, *6*(1), 131. https://doi.org/10.5194/soil-6-131-2020

Šantl-Temkiv, T., Finster, K., Dittmar, T., Hansen, B. M., Thyrhaug, R., Nielsen, N. W., & Karlson, U. G. (2013). Hailstones: A window into the microbial and chemical inventory of a storm cloud. *PLoS One*, *8*(1), e53550. https://doi.org/10.1371/journal.pone.0053550

Schirrmeister, L., Siegert, C., Kuznetsova, T., Kuzmina, S., Andreev, A., Kienast, F., et al. (2002). Paleoenvironmental and paleoclimatic records from permafrost deposits in the Arctic region of Northern Siberia. *Quaternary International*, *89*(1), 97–118. https://doi.org/10.1016/S1040-6182(01)00083-0

Schuur, E. A. G., Bockheim, J., Canadell, J. G., Euskirchen, E., Field, C. B., Goryachkin, S. V., et al. (2008). Vulnerability of permafrost carbon to climate change: Implications for the global carbon cycle. *BioScience*, *58*(8), 701–714. https://doi.org/10.1641/B580807

Schuur, E. A. G., McGuire, A. D., Schädel, C., Grosse, G., Harden, J. W., Hayes, D. J., et al. (2015). Climate change and the permafrost carbon feedback. *Nature*, *520*(7546), 171–179. https://doi.org/10.1038/nature14338

Simpson, A. J., Kingery, W. L., Hayes, M. H., Spraul, M., Humpfer, E., Dvortsak, P., et al. (2002). Molecular structures and associations of humic substances in the terrestrial environment. *Naturwissenschaften*, *89*(2), 84–88. https://doi.org/10.1007/s00114-001-0293-8

Spencer, R. G. M., Mann, P. J., Dittmar, T., Eglinton, T. I., McIntyre, C., Holmes, R. M., et al. (2015). Detecting the signature of permafrost thaw in Arctic rivers. *Geophysical Research Letters*, *42*(8), 2830–2835. https://doi.org/10.1002/2015GL063498

Strauss, J., Schirrmeister, L., Grosse, G., Fortier, D., Hugelius, G., Knoblauch, C., et al. (2017). Deep Yedoma permafrost: A synthesis of depositional characteristics and carbon vulnerability. *Earth-Science Reviews*, *172*, 75–86. https://doi.org/10.1016/j.earscirev.2017.07.007

Strauss, J., Schirrmeister, L., Grosse, G., Wetterich, S., Ulrich, M., Herzschuh, U., & Hubberten, H.-W. (2013). The deep permafrost carbon pool of the Yedoma region in Siberia and Alaska. *Geophysical Research Letters*, *40*(23), 6165–6170. https://doi.org/10.1002/2013GL058088

Stubbins, A., Mann, P. J., Powers, L., Bittar, T. B., Dittmar, T., McIntyre, C. P., et al. (2017). Low photolability of yedoma permafrost dissolved organic carbon: Low photolability of permafrost DOC. *Journal of Geophysical Research: Biogeosciences*, *122*(1), 200–211. https://doi.org/10.1002/2016JG003688

Stubbins, A., Spencer, R. G. M., Chen, H., Hatcher, P. G., Mopper, K., Hernes, P. J., et al. (2010). Illuminated darkness: Molecular signatures of Congo River dissolved organic matter and its photochemical alteration as revealed by ultrahigh precision mass spectrometry. *Limnology & Oceanography*, *55*(4), 1467–1477. https://doi.org/10.4319/lo.2010.55.4.1467

Stuiver, M. (1980). Workshop on $^{14}$C data reporting. *Radiocarbon*, *22*(03), 964–966. https://doi.org/10.1017/S0033822200010389

Stuiver, M., & Polach, H. A. (1977). Discussion reporting of $^{14}$C data. *Radiocarbon*, *19*(03), 355–363. https://doi.org/10.1017/S0033822200003672

Textor, S. R., Wickland, K. P., Podgorski, D. C., Johnston, S. E., & Spencer, R. G. M. (2019). Dissolved organic carbon turnover in permafrost-influenced watersheds of interior Alaska: Molecular insights and the priming effect. *Frontiers of Earth Science*, *7*. https://doi.org/10.3389/feart.2019.00275

Turetsky, M. R., Abbott, B. W., Jones, M. C., Anthony, K. W., Olefeldt, D., Schuur, E. A. G., et al. (2020). Carbon release through abrupt permafrost thaw. *Nature Geoscience*, *13*(2), 138–143. https://doi.org/10.1038/s41561-019-0526-0

Vasiliev, A. A., Drozdov, D. S., Gravis, A. G., Malkova, G. V., Nyland, K. E., & Streletskiy, D. A. (2020). Permafrost degradation in the Western Russian Arctic. *Environmental Research Letters*, *15*(4), 045001. https://doi.org/10.1088/1748-9326/ab6f12

Vonk, J. E., & Gustafsson, Ö. (2013). Permafrost-carbon complexities. *Nature Geoscience*, *6*(9), 675–676. https://doi.org/10.1038/ngeo1937

Vonk, J. E., Mann, P. J., Davydov, S., Davydova, A., Spencer, R. G. M., Schade, J., et al. (2013). High biolability of ancient permafrost carbon upon thaw. *Geophysical Research Letters*, *40*(11), 2689–2693. https://doi.org/10.1002/grl.50348

Vonk, J. E., Tank, S. E., Mann, P. J., Spencer, R. G. M., Treat, C. C., Striegl, R. G., et al. (2015). Biodegradability of dissolved organic carbon in permafrost soils and aquatic systems: A meta-analysis. *Biogeosciences*, *12*(23), 6915–6930. https://doi.org/10.5194/bg-12-6915-2015

Ward, C. P., & Cory, R. M. (2016). Complete and partial photo-oxidation of dissolved organic matter draining permafrost soils. *Environmental Science & Technology*, *50*(7), 3545–3553. https://doi.org/10.1021/acs.est.5b05354

Wickland, K. P., Waldrop, M. P., Aiken, G. R., Koch, J. C., Jorgenson, M. T., & Striegl, R. G. (2018). Dissolved organic carbon and nitrogen release from boreal Holocene permafrost and seasonally frozen soils of Alaska. *Environmental Research Letters*, *13*(6), 065011. https://doi.org/10.1088/1748-9326/aac4ad

Wild, B., Andersson, A., Bröder, L., Vonk, J., Hugelius, G., McClelland, J. W., et al. (2019). Rivers across the Siberian Arctic unearth the patterns of carbon release from thawing permafrost. *Proceedings of the National Academy of Sciences*, *116*(21), 10280–10285. https://doi.org/10.1073/pnas.1811797116

Williams, E. K., Rosenheim, B. E., Allison, M., McNichol, A. P., & Xu, L. (2015). Quantification of refractory organic material in Amazon mudbanks of the French Guiana Coast. *Marine Geology*, *363*, 93–101. https://doi.org/10.1016/j.margeo.2015.02.009

Williams, E. K., Rosenheim, B. E., McNichol, A. P., & Masiello, C. A. (2014). Charring and non-additive chemical reactions during ramped pyrolysis: Applications to the characterization of sedimentary and soil organic material. *Organic Geochemistry*, *77*, 106–114. https://doi.org/10.1016/j.orggeochem.2014.10.006

Zimov, S. A., Davydov, S. P., Zimova, G. M., Davydova, A. I., Schuur, E. A. G., Dutta, K., & Chapin, F. S. (2006). Permafrost carbon: Stock and decomposability of a globally significant carbon pool. *Geophysical Research Letters*, *33*(20). L20502. https://doi.org/10.1029/2006GL027484